Journal of Nuclear Materials 385 (2009) 527–532

Contents lists available at ScienceDirect

Journal of Nuclear Materials

journal homepage: www.elsevier.com/locate/jnucmat

Chemical corrosion and gamma-ray attenuation properties of Zr and Ti containing lead silicate glasses

Rafi Ali Rahimi [a,b], Gholamreza Raisali [c,*], S.K. Sadrnezhaad [b,d], Anita Alipour [e]

[a] Material Research School, Nuclear Science and Technology Research Institute, Atomic Energy Organization of Iran, P.O. Box 31485-498, Karaj, Iran
[b] Materials and Energy Research Center, P.O. Box 14155-4777, Tehran, Iran
[c] Radiation Applications Research School, Nuclear Science and Technology Research Institute, Atomic Energy Organization of Iran, End of Karegare Shomali Street, P.O. Box 11365-3486, Tehran, Iran
[d] Department of Material Science and Engineering, Sharif University of Technology, P.O. Box 11365-9466, Tehran, Iran
[e] Agricultural, Medical and Industrial Research School, Nuclear Science and Technology Research Institute, Atomic Energy Organization of Iran, P.O. Box 31485-498, Karaj, Iran

ARTICLE INFO

Article history:
Received 15 July 2008
Accepted 15 December 2008

ABSTRACT

Lead silicate glasses (LSGs) have high gamma-ray attenuation but low chemical durability properties. In this work, LSGs with (55.5–68.5 wt%) PbO content containing ZrO_2 and TiO_2 additions were produced. The chemical corrosion of various produced LSGs in 0.5 N HNO_3 aqueous solution and determination of their gamma-ray attenuation coefficients for ^{60}Co and ^{137}Cs sources were investigated. The weight loss measurements, the SEM micrographs, the EDS analysis of the sample surfaces and the ICP analysis of solution were used to characterize the dissolution process. The effects of PbO content, ZrO_2 and TiO_2 additives on chemical corrosion, and also the effect of PbO on gamma-ray attenuation coefficient, glass transition temperature (Tg), and density of LSG glasses were determined. The results showed that by increasing the lead content of glass the gamma-ray attenuation coefficient, chemical corrosion and density were increased, but the Tg decreased. One of the samples with PbO contents of 65.4 wt% and SiO_2 content of 26.9 wt% showed a very low chemical corrosion behavior and good gamma-ray absorption property.

1. Introduction

Addition of lead in silicate glass reduces the melting point and network connectivity, but increases the density, refractive index, chemical corrosion, electrical conductivity, and radiation attenuation coefficient of X- and gamma-rays [1–7].

The chemical corrosion of LSG glasses have been the object of several investigations [5–7]. In low lead content (<50 mol% PbO) LSG glasses, Pb has the network modifying role [1,3,4,6] which generates non-bonding oxygen atoms. These atoms are the most efficient in increasing the chemical corrosion of glass. When a piece of LSG glass is placed inside the aqueous acid solution, two distinct reactions occur. First, the ion-exchange is started by the reaction (1):

$$\equiv Si{-}O{-}Pb{-}O{-}Si\equiv + 2H^+ \leftrightarrow 2(\equiv Si{-}O{-}H) + Pb^{2+}. \quad (1)$$

The rate of this reaction is dependent on the lead content and the mass transport of lead and proton through Pb-depleted hydrated silica layer on glass surface [6–8]. The mass transport is reduced in presence of small amount of higher field strength cations such as Mg^{2+}, Ca^{2+}, Al^{3+}, Ti^{4+}, and Zr^{4+} in glass composition containing other modifiers [9–13].

Secondly, by taking place of the ion-exchange reaction which results in the production of Pb-depleted layer, the water diffusion and the water surface contact with sample are increased. Therefore, the water molecules penetrate through this layer and react with silica network by the hydrolysis reaction (2):

$$\equiv Si{-}O{-}Si\equiv + H_2O \leftrightarrow 2(\equiv Si{-}O{-}H). \quad (2)$$

This reaction, in more open silica network, occurs at a faster rate, breaks down the Si–O–Si bonds and leads to glass dissolution.

On the other hand, in physical point of view, the high amount of lead in these glasses makes them highly effective for attenuation of gamma-rays due to high atomic number and density of lead. Therefore, for radiation protection applications, investigation on determination of gamma-ray attenuation coefficients of these glasses is very important.

In this study, the effect of TiO_2 and ZrO_2 additives and the ratio of (Pb + Na + K)/Si of composition on chemical corrosion of LSGs samples were investigated. Also the density, glass transition temperature (Tg) and gamma-ray attenuation coefficients of these glasses were determined.

* Corresponding author.
E-mail addresses: rrahimi@nrcam.org (R.A. Rahimi), graisali@aeoi.org.ir, raisali@yahoo.com (G. Raisali), sadrnezh@sharif.edu (S.K. Sadrnezhaad), aalipoor@nrcam.org (A. Alipour).

0022-3115/$ - see front matter © 2009 Elsevier B.V. All rights reserved.
doi:10.1016/j.jnucmat.2008.12.046

2. Experimental procedure

2.1. Glass preparation

Lead silicate glasses were produced from technical grade silica (Iran, Hamedan), Pb_3O_4 (Iran) and reagent grade Na_2O, K_2O, ZrO_2, TiO_2 and As_2O_3 (Aldrich Chemical Co.) powders. Different glass compositions, with and without ZrO_2 and TiO_2 additives were produced for studying the chemical corrosion behavior in aqueous acid solutions. The chemical compositions of different samples are given in Table 1. Also this Table includes the analyzed Al_2O_3 values entered to glass due to melting in alumina crucible. For determination of the optimum amounts of ZrO_2 and TiO_2 additives, different values of these oxides given in Table 2 were added to the composition of S20 sample, separately. Two batches of the base composition of S20 were prepared and then, into one of these batches ZrO_2, and into the other TiO_2 is added as given in Table 2. Then the samples were melted separately according to the melting process given bellow.

A batch of each sample composition weighing 0.500 kg was mixed completely in a ceramic jar and melted in an alumina crucible in air and in an electric furnace (Exciton Co., Iran) at temperatures in the range of 1200–1300 °C for 2 h. For achieving better homogeneity, the glass melt were quenched into room temperature water. The generated frit was ground to >60 mesh and well mixed in a ceramic mortar. The treatments of quenching in water and grinding in mortar were repeated twice. The final ground glass powder was melted and poured in stainless steel moulds (Disk shape for gamma-ray attenuation and rectangular blocks for chemical corrosion tests). The samples annealed at about 10 °C above the glass transition temperature for 12 h. Then the furnace was turned off and cooled for about 15 h.

2.2. Dissolution tests

LSG glass compositions given in Tables 1 and 2 were used for dissolution experiments. The prepared lead silicate glass samples were cut into $0.015 \times 0.015 \times 0.003$ m^3 rectangular blocks with a diamond saw. One side of each sample was polished from rough to 3000 mesh with SiC papers. Other surfaces were isolated by an anti-acid paste (Sikagard 63 N, Sika and Sweis). The samples were degreased by rinsing in 2-propanol cleaning solution for three minutes before dissolution tests. Then washed with deionized water and dried at 60 °C for 4 h.

The dissolution tests were performed in 0.5 N HNO_3 (Ruth, Germany) aqueous solution at room temperature for 65 h. Also, the weight loss behavior of S30 and S3 samples in different periods of time was studied. Weight loss measurements were performed using Mettler Toledo AG204 balance with the accuracy of 10^{-7} kg for dissolution tests. The effect of TiO_2 and ZrO_2 additives and (Pb + Na + K)/Si ratio on the chemical corrosion of various glass compositions were investigated.

Characterization of the sample surfaces after dissolution experiments was carried out using a scanning electron microscope equipped with an EDS (Philips, XL30) probe. The atomic emission spectroscopy with an inductively coupled plasma measurements (ICP – Perkins Elmer Model Optima 2100 DV) determined the concentration of cations in solution after dissolution processes.

The weight loss of each glass sample was determined by measuring the surface area and the weight of samples before and after dissolution according to Eq. (3):

$$W_l = (W_i - W_f)/S, \tag{3}$$

where, W_l is the weight loss, W_i is the initial sample weight, W_f is the sample weight after dissolution experiment and S is the sample surface area.

Table 1
The composition of different produced lead glass samples in wt% (mol%) (the data obtained from two analysis uncertainty is 5%).

Sample*		PbO	SiO_2	ZrO_2	TiO_2	Na_2O	K_2O	As_2O_3	Al_2O_3
S10	wt%	55.8	37.7	–	–	1.5	2.6	0.3	2.1
	mol%	(26.3)	(66.0)	–	–	(2.5)	(2.9)	(0.2)	(2.2)
S20	wt%	65.6	30.2	–	–	0.5	1	0.3	2.2
	mol%	(35.1)	(60.0)	–	–	(1)	(1.3)	(0.2)	(2.6)
S30	wt%	68.5	27.5	–	–	0.5	1	0.3	2.2
	mol%	(38.7)	(57.7)	–	–	(1)	(1.3)	(0.2)	(2.7)
S1	wt%	55.6	34	2.4	1	1.6	2.8	0.3	2.3
	mol%	(26.9)	(61.2)	(2.1)	(1.4)	(2.8)	(3.2)	(0.2)	(2.3)
S2	wt%	65.4	26.9	2.4	1	0.6	1.2	0.3	2.2
	mol%	(35.8)	(54.7)	(2.4)	(1.5)	(1.2)	(1.6)	(0.2)	(2.6)
S3	wt%	68.5	24	2.4	1	0.6	1	0.3	2.2
	mol%	(39.3)	(51.1)	(2.5)	(1.6)	(1.2)	(1.4)	(0.2)	(2.8)

* Samples S10, S20, and S30 are the base compositions of S1, S2, and S3, respectively (without addition of TiO_2 and ZrO_2). The selection of this nomination is according to their equal PbO content.

Table 2
The amount of ZrO_2 and TiO_2 addition (in mol%) in the sample S20.

Additive	Sample					
	1	2	3	4	5	6
ZrO_2	0	0.8	1.6	2.4	3.2	–
TiO_2	0	0.4	0.8	1.2	1.6	2.0

2.3. Physical characterization

2.3.1. Density and glass transition temperature

The densities of the samples were determined using Archimedes principle. The samples were weighed using Mettler Toledo AG204 balance with the accuracy of 10^{-7} kg. Deionized water was selected as the immersing medium. The density was obtained from Eq. (4):

$$d = \frac{ax}{(a-b)}, \tag{4}$$

where 'a' is the weight of the glass in air, 'x' is the density of the inert immersion medium, and 'b' is the immersion weight of glass in deionized water. Thermal analysis was performed using Rheometric Scientific 1500 thermal analyzer (STA). The temperature scanned over a range from room temperature to 800 °C at uniform heating rate of 10 °C/min, for determination of glass transition temperature (Tg); the estimated error was ± 5 °C.

2.3.2. Gamma-ray attenuation

The attenuation coefficients of various lead content glasses were determined, according to the basic attenuation formula [14–17] given in Eq. (5)

$$I = I_0 e^{-\mu X}, \tag{5}$$

where, I_0 and I are gamma-ray intensities before and after passing through the sample with thickness of X and attenuation coefficient of μ, respectively.

Linear regression method was applied for determination of linear attenuation coefficients, using Eq. (6) obtained from Eq. (5):

$$\ln I = \ln I_0 - \mu X, \tag{6}$$

knowing that the negative of the slope of the regression line in a plot of ln I *versus* X is equal to μ.

The gamma-ray attenuation coefficients of various LSG compositions (for S1, S2, S3, and S30 samples given in Table 1) were

determined according to Eq. (6). The specimens with diameters of 0.080 m and thicknesses in the ranges from 0.005 to 0.020 m were polished by SiC stone. The measurements were performed in a good geometrical condition [15], for which the effect of scattered gamma rays from the sample and the laboratory was minimized as possible [16–18]. The good geometrical condition was established by using an indigenous designed and constructed collimator available at Iran National Secondary Standard Dosimetry Laboratory (SSDL). In addition, before performing the LSG sample measurements, the performance of the collimator was validated by measuring the attenuation coefficients of standard aluminum and copper samples with known values of attenuation coefficients at the desired energies [19–20].

The materials and equipments used in the measurements were as follows:

(1) ^{60}Co and ^{137}Cs gamma-ray sources (with average energy of 1.25 MeV for ^{60}Co and energy of 661 keV for ^{137}Cs).
(2) Multi stage collimator.
(3) Sample holder.
(4) Proportional counter (Berthold, model TOL-F) as gamma-ray detector.
(5) Detector shield.
(6) Calibration table with laser-equipped adjustment system.
(7) Aluminum and copper standard samples.

3. Results and discussion

3.1. Chemical corrosion

Fig. 1 shows the variation of weight loss as a function of different amounts of TiO_2 and ZrO_2 additives on samples with the base composition of S20. The amounts of additives are indicated in Table 2. This figure reveals that the weight loss decreases with addition of these oxides. Also this figure confirms that the effect of TiO_2 is more considerable on the weight loss.

Fig. 2 shows the variation of weight loss as a function of the ratio of the number of modifier cations per Si content of the samples (R = (Pb + Na + K)/Si). This figure reveals that the sample weight loss for (Pb + K + Na)/Si ratios up to 0.7 is negligible. The weight loss is significantly increased for (Pb + K + Na)/Si ratios higher than 0.7. Also this figure displays that the chemical durability of S1 and S2 samples is increased due to the addition of TiO_2 and ZrO_2.

The chemical corrosion behavior of LSG glasses containing TiO_2 and ZrO_2 additives and different amount of silica is affected by the bond and field strength of the cations in glass network. The bond strength (z/a) and field strength (z/a^2) values for charge 'z' and radius 'a' of different cations are indicated in Table 3. The bond strength in glass network points out to the ratio of ionicity and covalency of the bonds where it is often indicated by the field

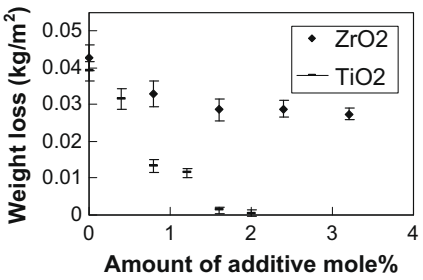

Fig. 1. The effect of TiO_2 and ZrO_2 addition on weight loss of the base sample S20, dissolved in 0.5 N HNO_3 acid solution.

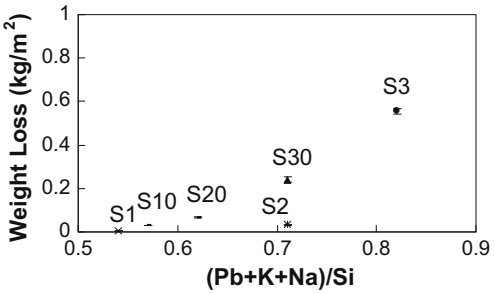

Fig. 2. Weight loss of different samples versus the ratio of (Pb + Na + K)/Si.

Table 3
The bond strength (z/a) and field strength (z/a^2) values of different cations in LSG glasses [9].

Strength	Cation							
	Si^{4+}	Ti^{4+}	Zr^{4+}	Al^{3+}	Pb^{2+}		K^+	Na^+
z/a	2.48	2.05	1.93	1.59	0.79	1.88	0.35	0.42
z/a^2	1.54	1.05	0.93	0.85	0.31	0.89	0.12	0.18

strength for better discrimination. The field strength values for the network former, modifier and intermediate cations are higher than 1.30, below 0.36 and between these two, respectively [9]. The Si^{4+} has the highest bond and field strength values which connects the network of silica strongly. The field strength of Zr^{4+}, Ti^{4+} and Al^{3+} cations are in intermediate range. K^+ and Na^+ cations are network modifiers. The Pb^{2+} has a dual role in the lead silicate network. It can be an intermediate cation or a network modifier depending on its content in the glass. Several researchers have reported that in lead silicate glasses with PbO content lower than 50 mol%, the lead atoms have the network modifying role [1,3,4,6]. From Table 1, it is obvious that the PbO content in all glass samples is lower than 40 mol%; therefore, it modifies the glass network in the prepared samples.

Chemical corrosion of the silicate glasses including lead silicate, involves two major processes: diffusion controlled ion-exchange and hydrolysis reactions of the silicate network. Presence of modifiers breaks down the direct connection of two silica tetrahedrons and connects them via the modifiers. For each connection of silica tetrahedrons via modifiers, one non-bonding oxygen atom (NBO) is produced. The ion-exchange reaction starts from the non-bonding oxygen atoms. Ion-exchange reaction rate is dependent on the content and mobility of the modifiers and proton through the glass network. The average number of the non-bonding oxygen atoms is calculated based on the assumption that one molecule of PbO generates one mole of NBO and one molecule of K_2O or Na_2O generates two moles of NBO. In the glass dissolution process, the ion-exchange reaction controls the initial dissolution of the glass, whereas the hydrolysis of the silica is responsible for the later stages of the dissolution. The transition time from ion-exchange to hydrolysis is relatively short in glasses with high amount of modifiers. In samples with higher modifier content, because of the extraction of upper modifier values, significant amount of nano-metric scale voids or porosity are created on surface of the samples during dissolution process. Generation of porosity multiplies the surface area of the sample exposing the solution and enhances the hydrolysis of silica. The ion-exchange reaction causes the leaching of the Pb^{2+}, K^+ and Na^+ cations. The mobility of these cations through glass network is restricted by the repulsive forces resulting from the electrostatic field strength of the network elements. Silicon atoms with higher field strength generate the strongest attractive force in (Si–O–Si) bonds and repulsive force against

Table 4
The leaching fraction 'LF(i)' of different cations of the samples.

Sample	LF(i)						
	LF(Na) $\times 10^{-6}$	LF(K) $\times 10^{-6}$	LF(Al) $\times 10^{-6}$	LF(Ti) $\times 10^{-6}$	LF(Zr) $\times 10^{-6}$	LF(Si) $\times 10^{-6}$	LF(Pb) $\times 10^{-6}$
S10	1596	1195	84		–	47	1074
S20	4792	3543	295	–	–	91	3270
S30	12584	9245	456	–	–	183	8756
S1	137	103	5	4	0	1.87	107
S2	794	625	67	54	21	28	581
S3	28113	24338	986	875	429	528	20741

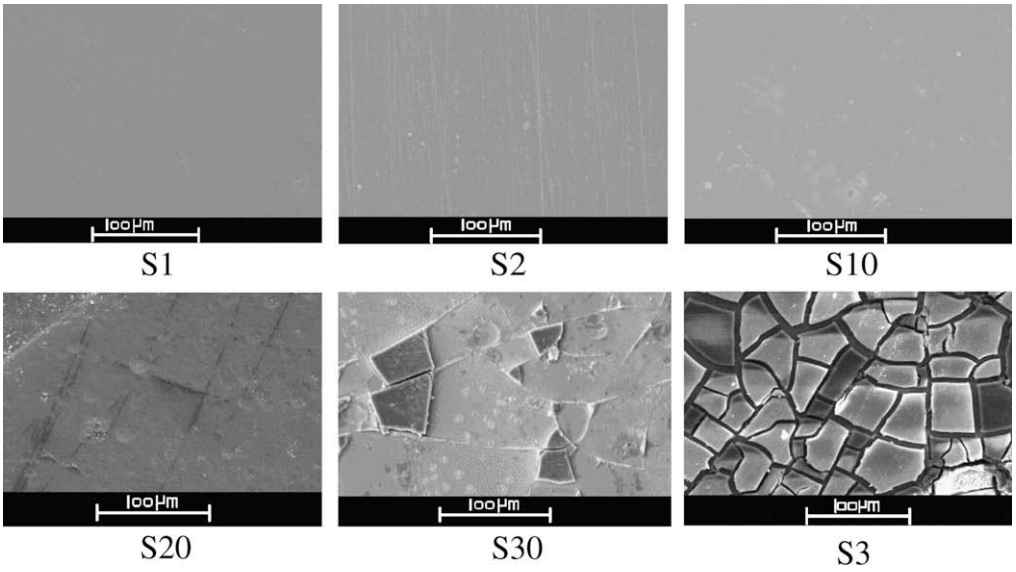

Fig. 3. SEM micrographs of the surface of different samples after dissolution.

migrating elements. The significant high field strength values of intermediates and their different size in relation to Si, not only do not deteriorate the connectivity of the network in high modifier content glasses, but also inhibit transfer of diffusing elements through the glass network.

The ICP analysis of different solutions after dissolution process was carried out to determine the leaching fraction 'LF(i)' of different cations in solution using Eq. (7):

$$LF(i) = \frac{C_i \times V}{f_i \times m}, \tag{7}$$

where C_i is the concentration of element i in solution, V is the volume of solution, f_i is the weight fraction of element i in the LSG sample and m is the LSG sample weight per unit area of the sample surface. The results of leaching fraction of different cations of the samples are given in Table 4. It demonstrates that the modifier content of solution is enhanced via increasing the lead content of the samples. The leaching fraction of Al and Ti is higher than Si and Zr. It points out that the hydrolysis of Al–O and Ti–O is faster than Si–O and Zr–O. Because of the same amount of aluminum oxide in all LSG samples or Ti–O in samples containing titanium oxide, the same amount of Al or Ti released into the solution. Hydrolysis of Al–O or Ti–O bonds enhances the porosity produced in ion-exchange reaction. The production of porosity multiplies the surface area, accelerates the water penetration through the porous hydrated layer and the hydrolysis rate of silica. It results in break down of silica network and enhances the weight loss. It should also be mentioned that the dissolution of samples with higher amount of Pb is more significant in the presence of aluminum and titanium oxide additives, due to higher initial porosity produced by the ion-exchange mechanism in high lead content glasses.

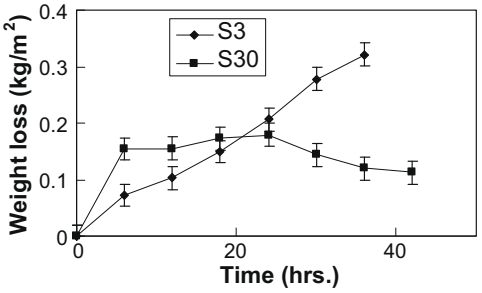

Fig. 4. The variation of weight loss as a function of time for S30 and S3 samples.

The presence of in-homogeneity in the samples composition due to un-sufficient mixing of raw material and glass melt during sample preparation process affects the chemical corrosion behavior of the samples and deteriorates the accuracy of the experiments. As mentioned in Section 2.1 (sample preparation), it has been tried to make more uniform composition of the samples. In order to examine the possibility of dissimilar corrosion of the samples, five probes for each composition were tested. Weight loss results showed good reproducibility. The SEM micrographs were also utilized at low magnification for analysis of the in-homogeneous corrosion of the samples surfaces. Fig. 3 shows the SEM micrographs of the samples after dissolution process. The surface morphology of the S1 does not illustrate any obvious change, but S2 and S10 exhibit some fine holes and linear grooves. In S20 the corrosion of the surface has been increased. In S3 and S30, the cracked

Table 5
EDS analysis of the surface of S30 and S3 samples (in wt%) before and after dissolution in 65 h.

Substance		Element							
		Na	K	Al	Si	Ti	Zr	Pb	O
S30	Before	0.87	1.00	2.46	13.07	–	–	67.40	15.20
	After	0.79	0.86	1.92	25.17	–	–	40.71	30.55
S3	Before	1.19	1.25	1.16	11.2	0.6	1.78	62.51	20.31
	After	0.91	1.03	1.47	13.91	0.94	2.98	60.78	17.98

Table 6
Density and R% (network connectivity percent) of different lead glass samples measured by Archimedes principle and calculated according to the chemical composition of samples, respectively.

Sample	Tg (°C)	Density (kg/m^3)
S10	492 ± 5	4170 ± 25
S20	497 ± 5	4795 ± 25
S30	473 ± 5	4820 ± 25
S1	525 ± 5	4390 ± 25
S2	534 ± 5	4880 ± 25
S3	512 ± 5	4940 ± 25

flaky deposits have been created on the surface of the samples. In all sample surfaces the distribution of decomposed regions are identical. It seems that the presence of any in-homogeneity and phase separation in the sample composition has been in the uncertainty ranges of SEM and weight loss measurements.

For attaining on higher information about chemical corrosion of S30 and S3 samples, some additional experiments were carried out in different periods of time. Fig. 4 shows the variation of weight loss of these samples as a function of dissolution time. It is linear for S3, but for S30, first, the weight loss increases and then remains approximately constant with increasing the dissolution time. The EDS analysis of the surface of S30 and S3 samples before and after dissolution process and removing of the gel layer is shown in Table 5. It illustrates that Pb-depleted silica rich layer has been produced on the surface of the S30 sample. Based on the weight loss behavior (Fig. 4) and the EDS analysis result (Table 5), it is concluded that the hydrolysis reaction controls the dissolution rate of the S3 and the ion-exchange reaction is a key factor in dissolution of S30 sample.

3.2. Density

The density and glass transition temperature (Tg) of all samples have been measured and are given in Table 6. Because of the high valence and small size of the silicon, silica tetrahedrons are connected on the corners resulting in large amount of free space between them. When Pb has a network modifying role in silica glass, it occupies the interstitial positions. Due to this phenomenon, negligible increase in the volume of silica network is obtained, but introducing high-density component (d_{PbO} = 9530 kg/m^3) [21] and reducing the low-density component (SiO_2) as another reason, increases the glass density.

Table 7
The values of the measured linear attenuation coefficients and mass attenuation coefficients of various samples for ^{137}Cs and ^{60}Co gamma-rays.

Sample	^{60}Co		^{137}Cs	
	μ (m^{-1})	μ/ρ (m^2/kg)	μ (m^{-1})	μ/ρ (m^2/kg)
S1	24.5 ± 0.6	0.00558	43.2 ± 0.6	0.00984
S2	28.0 ± 0.6	0.00574	49.2 ± 0.6	0.01008
S3	29.5 ± 0.6	0.00597	51.9 ± 0.8	0.01051
S30	27.7 ± 0.9	0.00575	50.0 ± 0.1	0.01037

3.3. Gamma-ray attenuation tests

The plot of ln (I/I_o) versus thickness of the S3 samples is shown in Fig. 5. Using the measured data and application of linear regression method, the linear and mass attenuation coefficient values of various samples are given in Table 7. The highest attenuation coefficient is for S3 samples (μ_1 = 29.5 ± 0.6 m^{-1} for ^{60}Co and μ_2 = 51.9 ± 0.8 m^{-1} for ^{137}Cs sources). The S2 samples exhibit very good chemical durability and also superior gamma-ray absorption property. Table 7 illustrates that due to enhancement of density and effective atomic number, the attenuation coefficient has been increased by PbO content of the glass. The measured attenuation coefficients are in good agreement with the recent values reported for high Pb silicate glasses [22].

4. Conclusion

In this work, the weight loss measurements, SEM micrograph of the surface of the samples and ICP analysis of the solutions were carried out for investigation on chemical corrosion of the samples. Also the gamma-ray attenuation coefficients, density and glass transition temperatures of different samples were determined. It was concluded that in LSG, the PbO content enhances the gamma-ray attenuation property and density but decreases the chemical durability and glass transition temperature. The chemical corrosion of various LSG samples exhibits different behaviors for different (Pb + K + Na)/Si values less than and greater than 0.7. Relatively higher content of silica in S1, S2, S10 and S20 samples, besides substitution of PbO by ZrO_2 and TiO_2 additives in minority

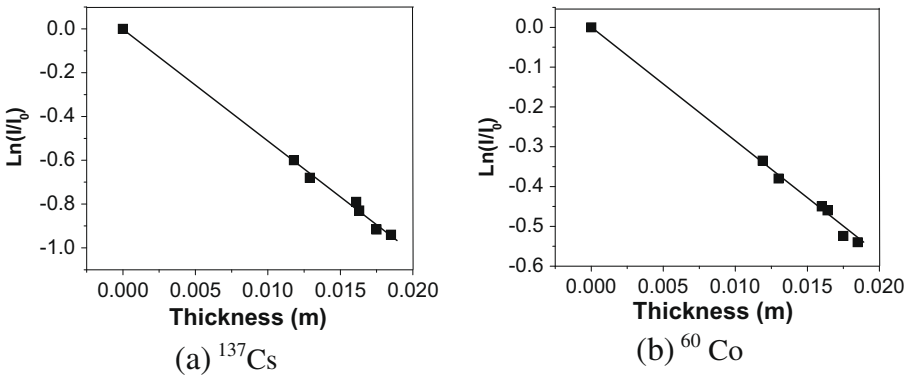

Fig. 5. Gamma-ray transmittance versus thickness for the S3 sample irradiated by: (a) ^{137}Cs, and (b) ^{60}Co gamma-rays.

in (S1, and S2) samples, improves the chemical durability. It seems that inhibiting the mobility of Pb and other modifying elements during ion-exchange reaction is a key factor for higher chemical durability of samples with (Pb + K + Na)/Si values lower than 0.7. In LSG glasses with higher Pb content, the production of porosity due to extraction of relatively large amount of modifiers, Al and Ti elements by means of hydrolysis, generates higher surface area against water molecules. In this situation, hydrolysis of silica bonds starts from silica tetrahedral with poor contacts on its similar neighbors. It seems that the dissolution of S3 is governed by hydrolysis and dissolution of S30 is governed by ion-exchange reactions. It is important to note that besides equal linear and mass attenuation coefficient and the modifiers to silicon ratio of S30 and S2 samples, the weight loss in S2 sample is negligible.

Acknowledgements

This investigation has been performed under financial support of Nuclear Science & Technology Research Institute. Authors wish to express their appreciation to F. Foroozanfar and A. Hamidi for the laboratory works, and also express their thanks to V. Ataeinia for the artworks.

References

[1] I.A. Weinstein, A.F. Zatsepin, V.S. Kortov, J. Non-Cryst. Solids 278 (2001) 77.
[2] A. Kanna, S.S. Bhatti, K.J. Singh, J. Mater. Sci. Let. 15 (1996) 815.
[3] F. Fayon, C. Landron, K. Sakurai, Bessada, C.D. Massiot, J. Non-Cryst. Solids 243 (1999) 39.
[4] U. Hoppe, R. Kranold, A. Ghosh, C. Landron, J. Neuefeind, P. Jovari, J. Non-Cryst. Solids 328 (2003) 146.
[5] A.A. Ahmed, I.M. Youssof, Glass Technol. 38 (1997) 30.
[6] C. Schultz –Münzenberg, W. Meisel, P. Gütlich, J. Non-Cryst. Solids 238 (1998) 83.
[7] C. Bonnet, A. Bouquillon, S. Turrell, V. Deram, B. Mille, J. Salomon, J.H. Thomassin, C. Fiaud, J. Non-Cryst. Solids 323 (2003) 214.
[8] M.J. Hynes, S. Forde, B. Jonson, The Sci. Total Environ. 319 (2004) 39–52.
[9] M.B. Volf, Chemical Approach to Glass, Elsevier Science Publishers, 1000 AE Amsterdam, Netherlands, 1984.
[10] B. Roling, M.D. Ingram, J. Non-Cryst. Solids 265 (2000) 113.
[11] R. Kirchheim, J. Non-Cryst. Solids 328 (2003) 157.
[12] H. Wakabayashi, J. Non-Cryst. Solids 203 (1996) 274.
[13] N.P. Bansal, R.H. Doremus, Handbook of Glass Properties, Materials Engineering Department, Rensselaer Polytechnic Institute, Troy, New York, 1986.
[14] H. Baltaş, Ş. Çelik, U. Çevik, E. Yanmaz, Radiat. Measure. 42 (2007) 55.
[15] G.F. Knoll, Radiation Detection and Measurement, 3rd Ed., John Wiley & Sons Inc., 1999.
[16] J.M. Wyckoff, H.W. Koch, Phys. Rev. 117 (1960) 1261.
[17] C.T. Chatler, C.Q. Tran, Z. Barnea, D. Paterson, D.J. Cookson, D.X. Balaic, Phys. Rev. A 64 (2001) 64.
[18] G.S. Sidhu, K. Singh, P.S. Singh, G.S. Mudahar, Radiat. Phys. Chem. 56 (1999) 535.
[19] M.J. Berger, J.H. Hubbell, NIST Standard Reference Database 8, Version 3.1, June, 1999.
[20] ICRU Report 44, X-ray Mass Attenuation Coefficients, 1989.
[21] H.B. George, C. Vira, C. Stehle, J. Meyer, S. Evers, D. Hogran, S. Feller, M. Affatigato, Phys. Chem. Glass. 40 (1999) 326.
[22] K.J. Singh, N. Singh, R.S. Kaudal, K. Singh, Nucl. Instr. Meth. Phys. Res. B 266 (2008) 944–948.